ACS Catalysis

pubs.acs.org/acscatalysis Research Article

Biochemical and Metabolic Insights into Hyoscyamine Dehydrogenase

Fei Qiu,[⊥] Yijun Yan,[⊥] Junlan Zeng,[⊥] Jian-Ping Huang, Lingjiang Zeng, Wei Zhong, Xiaozhong Lan, Min Chen, Sheng-Xiong Huang,* and Zhihua Liao*

Cite This: *ACS Catal.* 2021, 11, 2912−2924 Read Online

ACCESS | Metrics & More | Article Recommendations | Supporting Information

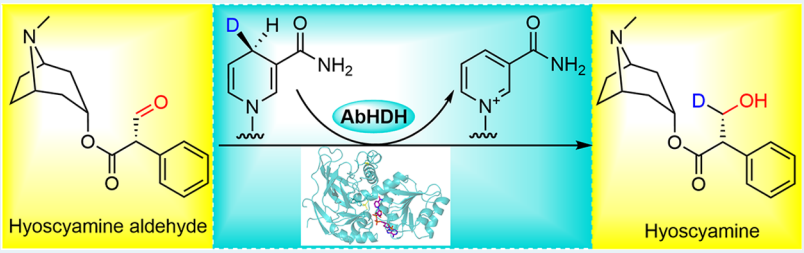

ABSTRACT: Hyoscyamine, a member of the class of compounds known as tropane alkaloids (TAs), is clinically used as an anticholinergic drug. Previous research has predicted that hyoscyamine is produced via the reduction of hyoscyamine aldehyde. In this study, we identified a root-expressed gene from *Atropa belladonna*, named *AbHDH*, which encodes a hyoscyamine dehydrogenase involved in the formation of hyoscyamine. Enzymatic assays indicated that AbHDH was able to not only reduce hyoscyamine aldehyde to produce hyoscyamine but also oxidize hyoscyamine to form hyoscyamine aldehyde under different conditions. To elucidate its catalytic mechanism, the crystal structure of AbHDH at a 2.4-Å resolution was also determined. Overexpression of *AbHDH* significantly enhanced the biosynthesis of hyoscyamine and the production of anisodamine and scopolamine in root cultures of *A. belladonna*. However, suppression of *AbHDH* using RNAi technology did not reduce the production of hyoscyamine, anisodamine, or scopolamine, though it did increase the accumulation of hyoscyamine aldehyde. In summary, this study provided timely biochemical and metabolic insights into hyoscyamine dehydrogenase, pointing to an alternative, promising way to produce pharmaceutical TAs via metabolic engineering in planta.

KEYWORDS: *biosynthesis, crystal structure, hyoscyamine, hyoscyamine dehydrogenase, metabolic engineering*

INTRODUCTION

Hyoscyamine is a tropane alkaloid (TA) that displays anticholinergic activity and is used clinically as a drug to treat various health disorders such as arrhythmias, organophosphate poisoning, and Parkinson's symptoms.[1] However, medicinal plants of the Solanaceae family, such as *Atropa belladonna*, *Duboisia* hybrid, and *Datura* spp., among others, are the only naturally occurring materials currently available for the commercial production of hyoscyamine.[2−4] Moreover, the levels of hyoscyamine in these plants are generally very low, strongly limiting its plant-based production for use in clinical applications.[5] Two Nobel laureates, Professor Richard Willstätter (1872−1942) and Sir Robert Robinson (1886−1975), made great contributions toward the chemical synthesis of this alkaloid.[6] Chemical synthesis of hyoscyamine is undoubtedly a great success of science, but it fails in the marketplace because this process is too costly. Plant breeders used genetic, radiant, and polyploidy breeding methods to attempt to develop new plant varieties distinguished by high yields of hyoscyamine, but all of these efforts failed.[5] However now that the TA biosynthetic pathway has been elucidated, metabolic engineering and synthetic biology offer new hope for engineering the production of hyoscyamine.

Although the biosynthesis of TAs constitutes a century-old unresolved problem,[6] substantial progress on this front has been made in recent years (Figure 1).[7,8] Putrescine, produced from an ornithine-decarboxylase-catalyzed decarboxylation of ornithine,[9] is a precursor for the biosynthesis of polyamines, nicotine, and TAs. In these biosynthesis, first putrescine *N*-methyltransferase (PMT) catalyzes the *N*-methylation of putrescine, to form *N*-methylputrescine;[10] next, *N*-methylputrescine oxidase (MPO) catalyzes the oxidative deamination of *N*-methylputrescine to produce 4-methylaminobutanal, which undergoes spontaneous cyclization to form the *N*-methyl-Δ^1-pyrrolinium cation.[11] The type III polyketide synthase (PYKS)

Received: October 27, 2020
Revised: February 6, 2021
Published: February 18, 2021

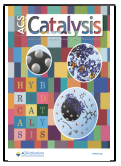

https://dx.doi.org/10.1021/acscatal.0c04667
ACS Catal. 2021, 11, 2912−2924

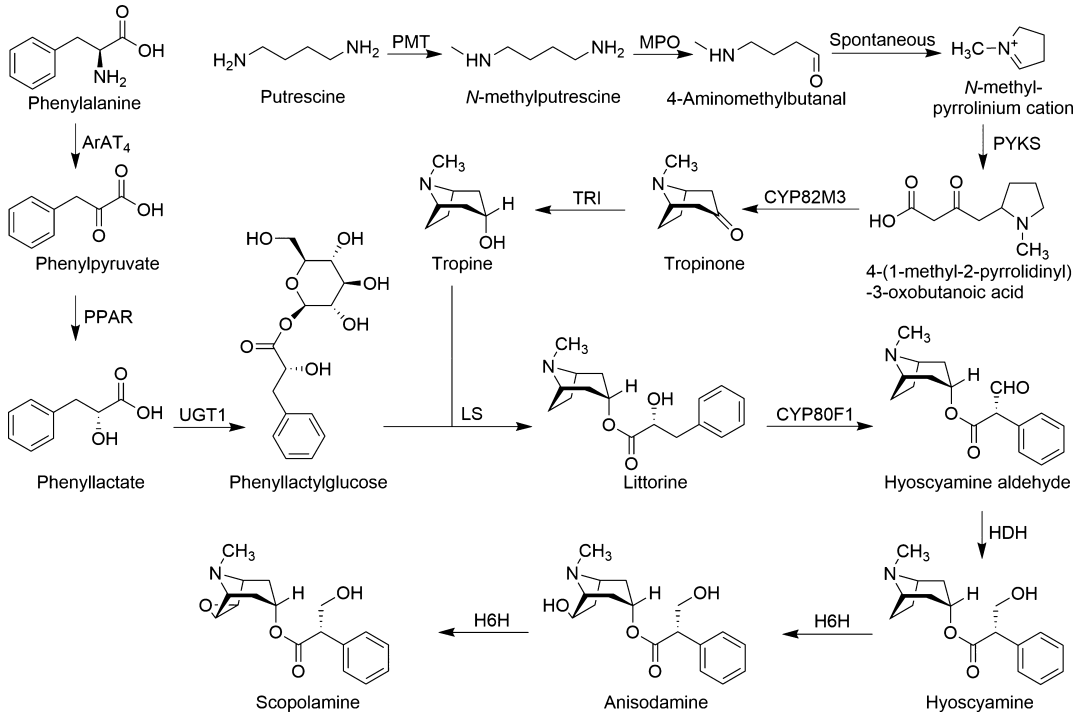

Figure 1. Biosynthetic pathway of tropane alkaloids in *Solanaceae*. PMT, putrescine *N*-methyltransferase. MPO, *N*-methylputrescine oxidase. PYKS, type III polyketide synthase. CYP82M3, tropinone synthase. TRI, tropine-forming reductase. UGT1, phenyllactate UDP-glycosyltransferase. ArAT4, aromatic amino acid aminotransferase. PPAR, phenylpyruvic acid reductase. LS, littorine synthase. CYP80F1, littorine mutase. HDH, hyoscyamine dehydrogenase. H6H, hyoscyamine 6β-hydroxylase.

converts this cation to 4-(1-methyl-2-pyrrolidinyl)-3-oxobutanoic acid, which is subsequently converted by CYP83M3 to form tropinone.[12,13] Tropine-forming reductase (TRI) reduces tropinone to tropine, which is used as an acyl acceptor for the formation of littorine.[14] Aromatic amino acid aminotransferase (ArAT4) then catalyzes the formation of phenylpyruvic acid, by using phenylalanine as a substrate.[15] Phenylpyruvic acid reductase (PPAR) catalyzes the reduction of phenylpyruvic acid to phenyllactic acid,[16] which is further converted by UDP-glycosyltransferase (UGT1) to phenyllactylglucose as the acyl donor for littorine formation.[7] Then, littorine synthase (LS) catalyzes the esterification of tropine (the acyl acceptor) with phenyllactylglucose (the acyl donor) to produce littorine.[7] Finally, littorine mutase (CYP80F1) catalyzes the rearrangement of littorine into hyoscyamine aldehyde (HYA).[17] It was postulated a while ago that an alcohol dehydrogenase, unidentified at that point, might be responsible for catalyzing the formation hyoscyamine via the reduction of HYA.[18,19] Two recent studies reported on a hyoscyamine-producing alcohol dehydrogenase, named HYA reductase (HAR) in our patent[20] or hyoscyamine dehydrogenase (HDH),[8] identified from two hyoscyamine-producing plants, namely *A. belladonna* and *Datura stramonium*, respectively. With the discovery of HDH (or HAR), all of the functional genes involved in hyoscyamine biosynthesis have now been identified. Hyoscyamine 6β-hydroxylase (H6H) catalyzes the 6β-hydroxylation of hyoscyamine, to generate anisodamine, and this same enzyme subsequently also catalyzes the epoxidation of anisodamine to form scopolamine.[21,22]

HDH, as the last identified gene in TA biosynthesis, has been used to manufacture hyoscyamine and scopolamine in yeast by implementing synthetic biology technologies.[8] This biosynthesis of pharmaceutical TAs in yeast represents a great milestone in the field of synthetic biology. However, the biochemistry of HDH remains poorly understood, and its role in TA biosynthesis is also unknown in planta; furthermore, the value of HDH for engineering hyoscyamine production has not been studied in TA-producing plants. To address these gaps in knowledge, the *HDH* gene of *A. belladonna* (hereon *AbHDH*) was in the current work studied at the molecular, biochemical, and structural levels. Here, *AbHDH* was overexpressed to estimate its potential contribution to engineering the production of hyoscyamine, anisodamine, and scopolamine in root cultures of *A. belladonna*. Also, in planta, *AbHDH* was suppressed using RNAi technology to investigate its functional role in hyoscyamine biosynthesis. Our suite of experiments has yielded a sounder understanding of HDH at the biochemical level, and the results have provided an alternative and competitive way to metabolically engineer the production of hyoscyamine, anisodamine, and scopolamine in plant materials. Finally, we anticipate that our findings will also spur scientists to think more about the complexity of the process by which hyoscyamine is formed in planta.

RESULTS AND DISCUSSION

Gene Cloning and Expression Analysis. HYA provided by CYP80F1 was postulated to be the direct precursor for hyoscyamine formation,[17] leading several scientists to propose that alcohol dehydrogenase might catalyze the reduction of HYA to form hyoscyamine.[19,23] The alcohol dehydrogenase (ADH) conserved domain (PF08240) was used to search the *A. belladonna* transcriptomes, and 31 unigenes were identified (Table S1). TAs are synthesized in secondary roots, in which the known TA biosynthesis genes are specifically, or highly, expressed,[7,12,15,16,24] and such a root-expressed pattern leads to postulate the candidate alcohol dehydrogenase responsible for

https://dx.doi.org/10.1021/acscatal.0c04667
ACS Catal. 2021, 11, 2912−2924

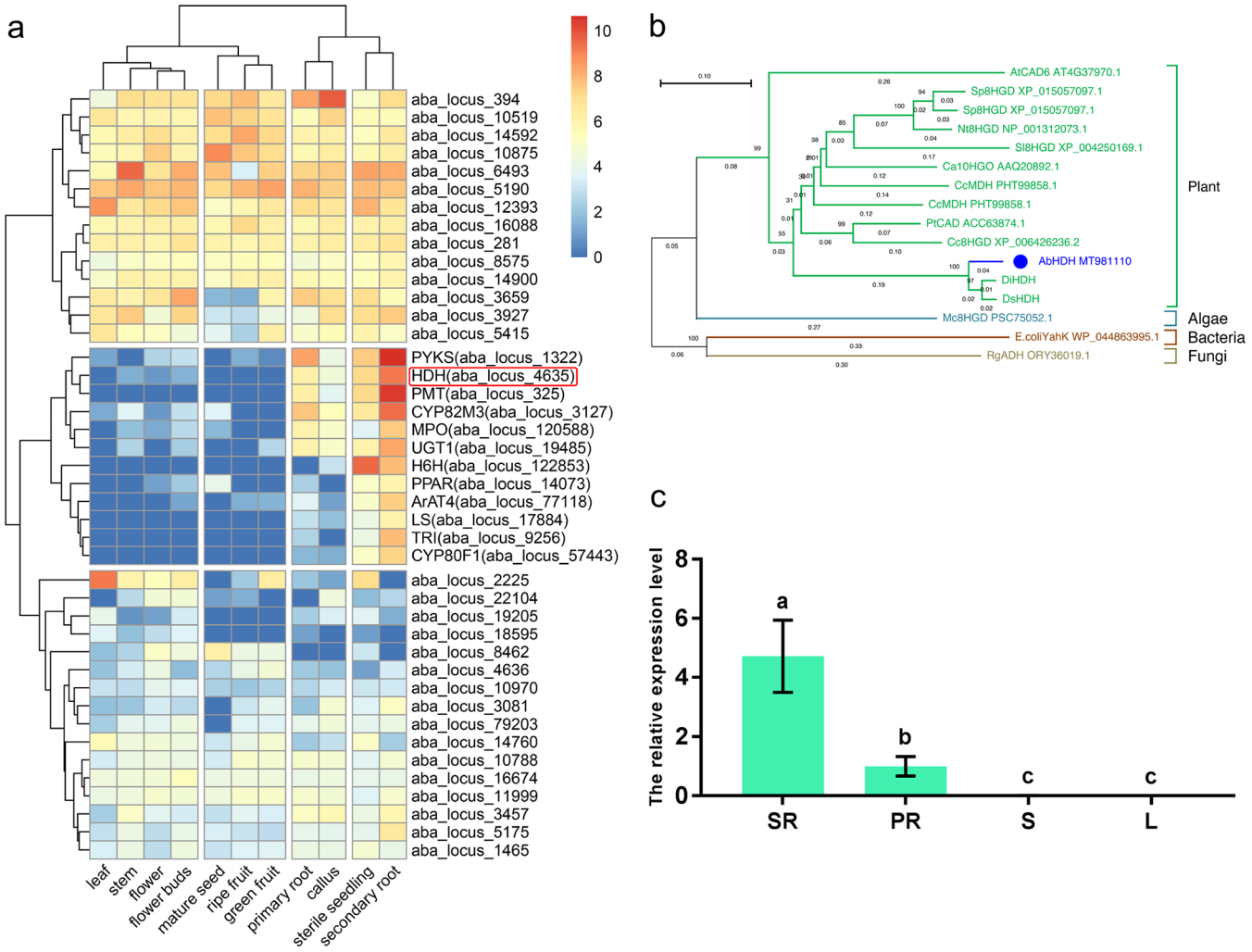

Figure 2. Bioinformatics and tissue expression analysis of *HDH*. (a) Digital gene expression patterns of alcohol dehydrogenase and TA biosynthesis genes from transcriptomes of *A. belladonna* in its plant tissue types. (b) The constructed phylogenetic tree of the ADH proteins. (c) Expression levels of *HDH* in secondary root (SR), primary root (PR), stem (S), and leaf (L) tissues. The bars on the columns show the respective standard deviations (n = 3). Tissues labeled with different letters (a−c) above the columns showed significant differences in HDH expression levels (P < 0.05, as determined by Duncan's test).

hyoscyamine formation might be specifically or highly expressed in secondary roots. Of the 31 ADH genes, just one (aba_locus_4635) showed a tissue expression profile similar to that of the characterized TA biosynthesis genes (Figure 2a). Hence, aba_locus_4635 was considered to be the only candidate gene for hyoscyamine dehydrogenase. The cDNAs of *AbHDH* were cloned and deposited into GenBank (under accession number MT981110). A phylogenetic analysis indicated that plant and microbial or algae alcohol dehydrogenases could be divided into different clades (Figure 2b). Three HDHs (AbHDH, DsHDH and DiHDH) were grouped to form a subclade separated from plant alcohol dehydrogenases (Figure 2b), suggesting an evolutionary and functional divergence between HDHs and plant alcohol dehydrogenases. AbHDH and DsHDH/DiHDH were found to display 93.7%/93.2% amino acid sequence identity. These results showed the three HDHs sharing a common ancestor. Digital gene expression analysis revealed a tissue profile for *AbHDH* similar to the tissue profiles of known TA biosynthesis genes. The expression levels of *AbHDH* in four representative tissues, namely secondary roots, primary roots, stems, and leaves, were determined using the real-time quantitative polymerase chain reaction (qPCR; Figure 2c) and indicated that *AbHDH* was highly expressed in the *A. belladonna* secondary roots, moderately expressed in the primary roots, but not expressed in the stems or leaves.

Hyoscyamine Dehydrogenase Catalyzes the Reciprocal Conversion between HYA and Hyoscyamine. The His-tagged HDH protein was produced in engineered *Escherichia coli* and purified using Ni^{2+}-resin columns. SDS-PAGE showed AbHDH at the apparent molecular weight of 42.9 kDa (Figure S1), a value consistent with its calculated molecular weight. Due to the very low stability of HYA and, as a result, its high susceptibility to quickly undergoing the retro-Claisen condensation reaction, it is neither commercially available nor at all easy to produce in the laboratory. Therefore, here, successive reactions were used to identify the reduction activity of AbHDH. First, the upstream *CYP80F1* gene of *A. belladonna* was ectopically expressed in the yeast strain WAT11, which has been successfully used to identify catalytic functions of cytochrome P450s.[25−27] When littorine was fed to microsomal proteins with CYP80F1, HYA (m/z 288.1586; Figure S2) was detected and identified (Figure 3a). These results were consistent with those reported by Li et

https://dx.doi.org/10.1021/acscatal.0c04667
ACS Catal. 2021, 11, 2912−2924

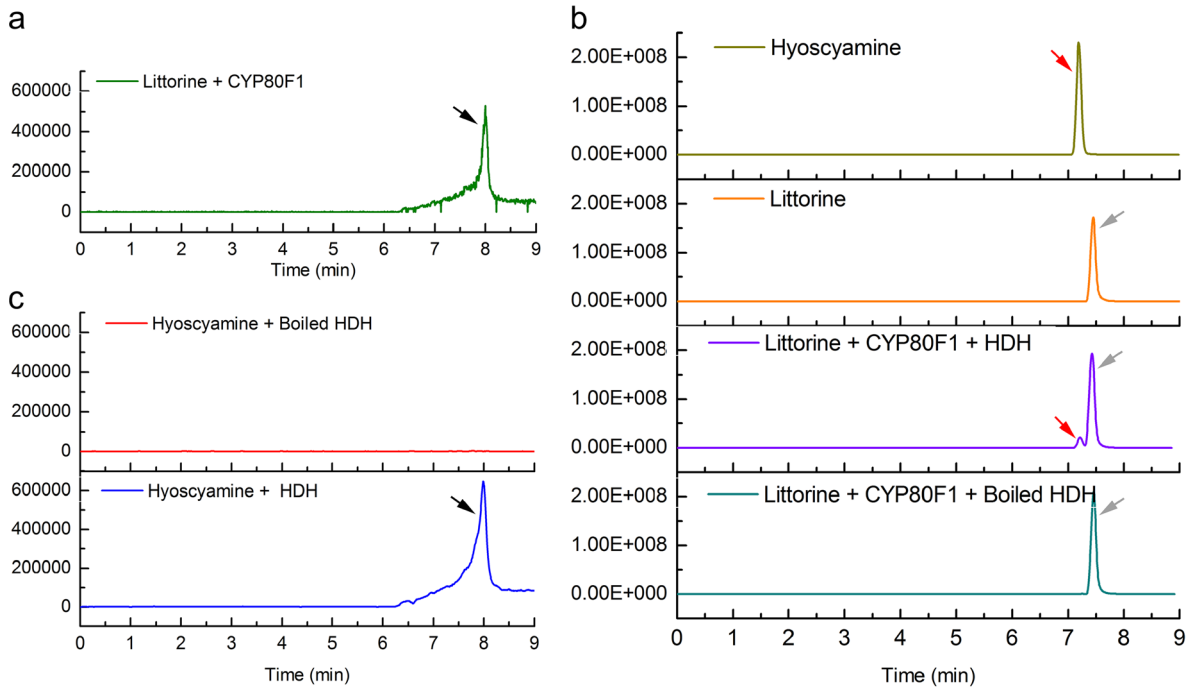

Figure 3. HDH enzymatic assays. (a) Extracted-ion chromatogram (EIC) trace of the CYP80F1-mediated littorine carbon rearrangement. (b) EIC traces of the AbHDH-mediated reduction reaction system. Here, dark yellow and orange lines represent authentic samples of hyoscyamine and littorine, respectively; the violet line indicates the detected metabolites in the reaction system containing littorine, CYP80F1, and purified HDH protein; and the dark cyan line shows the detected metabolites in the reaction system containing littorine, CYP80F1 and boiled HDH protein, as a negative control. (c) EIC traces of the HDH-mediated oxidation reaction system. Here, the red line indicates the detected metabolites in a negative control using boiled HDH; and the blue line shows the detected metabolites in the HDH-mediated hyoscyamine oxidation reaction. Black arrows indicate HYA, red arrows represent hyoscyamine, and gray arrows show littorine. The *X*-axis represents retention time, and the *Y*-axis represents the relative abundance.

al.[17] Hyoscyamine (m/z 290.1742; Figure S3) was produced when the purified His-tagged HDH protein was added into the reaction system for the purpose of producing HYA (Figure 3b), and hyoscyamine was not detected in a boiled AbHDH control (Figure 3b). These results demonstrated the ability of AbHDH to reduce HYA, to form hyoscyamine, in a cell-free reaction system producing HYA. When hyoscyamine was used instead as the substrate, the formation of HYA (m/z 288.1585; Figure S4) was detected (Figure 3c). Biochemical analysis revealed AbHDH functioning as an oxidoreductase, i.e., not only reducing HYA to hyoscyamine, but also oxidizing hyoscyamine to HYA.

Structural Features of AbHDH and Its Binding of Substrate. To determine the structural basis for the catalytic mechanism of AbHDH, its crystal structure was determined to a resolution of 2.4 Å (Protein Data Bank [PDB] ID: 7CGU; Table S2). An amino acid sequence alignment indicated the structure of AbHDH to be similar to that of heteroyohimbine alkaloid synthase (PDB ID: 5H81 and 5FI3) and[28] cinnamyl or sinapyl alcohol dehydrogenase (PDB ID: 2CF5, 5VKT, and 1YQD;[29−31] Figure S5). Inspection of the crystal structure showed the AbHDH monomer consisting of two domains, with one of them being a nucleotide-binding domain consisting of a classic Rossman fold and the other domain being a substrate-binding domain. Figure 4a shows the overall structure of AbHDH, with its active sites defined by NADP(H) cofactor, a catalytic Zn^{2+}, and a deep cavity formed between the two domains. Like those of many members of the zinc-dependent CAD or SAD family, the active sites cavity of AbHDH was observed to contain a catalytic zinc sphere, with the zinc coordinated by one histidine (His74), one glutamate (Glu75), and two cysteines (Cys52 and Cys168) and together showing approximate tetrahedral symmetry (Figure 4b). Atop the active site cavity, three nonpolar residues—Met124, Leu282, and Ala305—together formed a substrate-binding pocket that, much like three fingers, would appear to control the HYA substrate binding via shape-dependent van der Waals interactions (Figure 4c). Furthermore, deep in the pocket, the two polar residues Ser54 and Cys100 may have formed a critical hydrogen bond with the carbonyl oxygen of aldehyde (Figure 4c).

Because of the difficulty in obtaining ternary complex crystals for AbHDH, a computational docking program, namely AutoDock,[32] was used to probe the structural basis of substrate binding in AbHDH. Judging by the inferred conformations and binding affinities, the most favorable orientation of the HYA as well as that of phenylacetaldehyde, each in the AbHDH active site, was determined as shown in Figures 4d and S6a respectively. The docking results showed the binding profile of the benzene ring and aldehyde group of phenylacetaldehyde to be very similar to the binding profile of the corresponding groups of HYA (Figure S6b). In the docked conformation of HYA, the distances from the HYA oxygen to the catalytic Zn^{2+}, the hydroxyl side chain of Ser54, and the sulfhydryl side chain of Cys100 were measured to be 3.7, 2.8, and 3.3 Å, respectively (Figure 4e). In addition, the carbonyl carbon of the HYA was measured to be situated 3.5 Å away from the C4 atom of the nicotinamide ring of the bound NADP(H) molecule, which showed the *pro*-R hydrogen in an

https://dx.doi.org/10.1021/acscatal.0c04667
ACS Catal. 2021, 11, 2912−2924

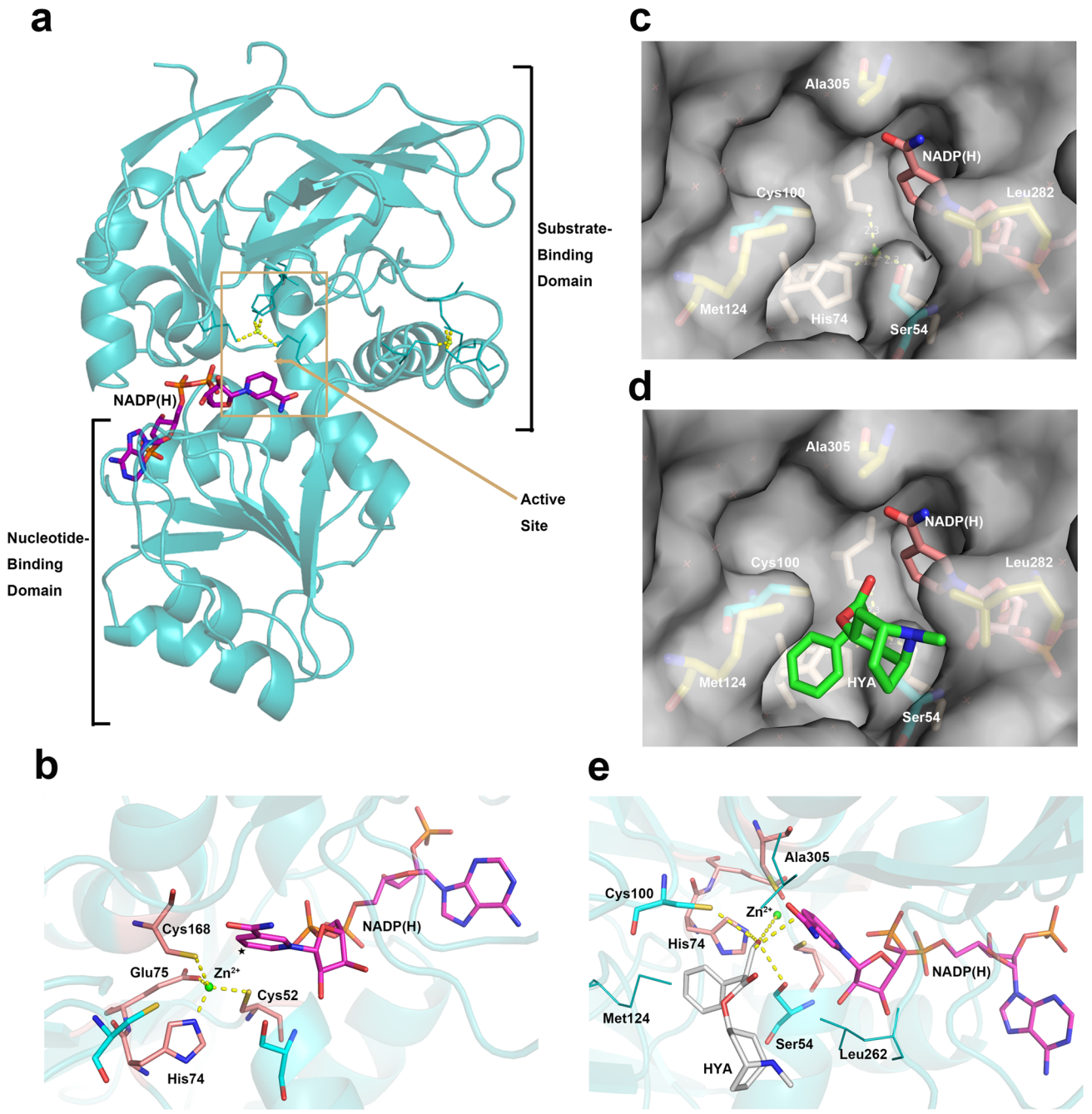

Figure 4. Structure of AbHDH. (a) Cartoon representation of the AbHDH monomer (colored teal), with NADPH bound to its nucleotide-binding domain. The location of the active site cavity is indicated by a yellow rectangle. The AbHDH monomer was observed to coordinate one structural and one catalytic Zn^{2+} ion, each depicted here as a green sphere with small yellow spheres indicating the coordination bonds. (b) Cartoon and stick representation of the AbHDH active site. The catalytic Zn^{2+} ion, observed to be tetrahedrally coordinated by Cys52, His74, Glu75, and Cys168, is depicted here as a green sphere. Small yellow spheres indicate the coordination bonds formed between the Zn^{2+} ion and the residues. A stick model of NADPH is shown. The site of hydride transfer is labeled with an asterisk. (c) Surface representation of the substrate-binding pocket. (d) Surface representation of the binding pocket docked with HYA. (e) Cartoon and stick representation of the AbHDH active site cavity docked with HYA. Six residues constituting the substrate-binding pocket are indicated. The docking suggested formation of a hydrogen bond between the carbonyl group of HYA and the Ser54 residue, postulated to be the key catalytic residue of AbHDH.

appropriate position for ensuring the hydride transfer (Figure 4e).

Enzyme Kinetics and Reaction Mechanism. Unlike the reduction reactions catalyzed by some zinc-dependent CAD or SAD family protein members, the reduction reaction catalyzed by AbHDH is reversible.[31] Here we relied on hyoscyamine to derive the enzyme kinetics of this reverse reaction. Furthermore, we found that AbHDH can reduce various HYA mimics, such as phenylacetaldehyde (Figure S7). Therefore, enzyme kinetics assays with the wild type and mutants were carried out in the presence of phenylacetaldehyde for the reduction reaction, and likewise with hyoscyamine for the reverse reaction. The optimized pH level and temperature for the AbHDH-catalyzed reduction were, respectively, 6.4 and 40 °C (Figure S8). Under these optimal conditions, the *Km* value of the wild-type AbHDH for

https://dx.doi.org/10.1021/acscatal.0c04667
ACS Catal. 2021, 11, 2912−2924

Table 1. Enzymatic Kinetics Parameters of Wild-Type AbHDH and Five Mutants[a]

kinetic parameters	wild-type AbHDH	S54A	H74A	C100G	C100Y	C100F
phenylacetaldehyde						
K_m (μM)	44.46 ± 10.73	n.d.	n.d.	199.8 ± 45.77	357.3 ± 83.33	492.4 ± 178.6
k_{cat} (min^{-1})	228.4 ± 21.39	n.d.	n.d.	7.14 ± 0.89	2.83 ± 0.40	3.79 ± 0.91
k_{cat}/K_m (min^{-1} μM^{-1})	5.14	n.d.	n.d.	0.036	0.008	0.008
hyoscyamine						
K_m (μM)	33.36 ± 4.69	285.9 ± 73.36	n.d.	21.69 ± 3.19	485.5 ± 154.6	937.4 ± 258.4
k_{cat} (min^{-1})	7.49 ± 0.51	0.62 ± 0.04	n.d.	1.47 ± 0.09	0.28 ± 0.04	0.52 ± 0.09
k_{cat}/K_m (min^{-1} μM^{-1})	0.22	0.002	n.d.	0.068	0.0006	0.0006

[a]n.d., enzyme reaction not detected.

phenylacetaldehyde was 44.46 ± 10.73 μM, and its corresponding k_{cat} and k_{cat}/K_m values were 228.4 ± 21.39 min^{-1} and 5.14 min^{-1} μM^{-1}, respectively (Table 1). The reverse reactions (i.e., oxidation activity) of AbHDH, using hyoscyamine and phenylethanol as substrates, were also analyzed. Maximum activity of AbHDH-mediated oxidation of hyoscyamine was detected at pH 10.4 and 45 °C (Figure S8). Under these conditions, the K_m value of AbHDH for hyoscyamine was 33.36 ± 4.69 μM, for which the k_{cat} and k_{cat}/K_m values were, respectively, 7.49 ± 0.51 min^{-1} and 0.22 min^{-1} μM^{-1} (Table 1); however, there was no activity when phenylethanol served as the substrate. Under optimal conditions, the reduction efficiency of HDH was 23.36 times that of its oxidation efficiency. Specifically, the catalytic efficiency of HDH associated with reduction was much higher than that with oxidation under optimal conditions (Table 1), and the equilibrium constants of the reactions at pH 6.4, 7.2, and 10.4 when hyoscyamine was used as the substrate were 5323.82, 915.06, and 12.57 respectively. These results suggested that HDH is more prone to reducing aldehyde to alcohol rather than oxidizing alcohol to aldehyde under physiological conditions of plants (around pH 7.2).

To investigate the role of key catalytic residues in the functioning of the active site pocket of AbHDH, five mutants (S54A, H74A, C100G, C100Y, and C100F) were generated through site-directed mutagenesis. The H74A site mutation led to loss of enzyme activity for each of the two tested substrates (Table 1); enzyme activity profiles of C100G showed only 0.70% of the wild-type activity for phenylacetaldehyde and 30.90% of the wild-type activity for hyoscyamine, and both C100Y and C100F showed only 0.16% and 0.27% of the wild-type activity for phenylacetaldehyde and hyoscyamine, respectively (Table 1). By contrast, mutant S54A displayed no catalytic activity at all when using phenylacetaldehyde as the substrate; and when hyoscyamine was used as the substrate, its activity amounted to just 0.91% of that of the wild type (Table 1), highlighting the key participation of Ser54 for a successful HDH-catalyzed aldehyde reduction. The highly reduced catalytic activity of HDH for the Ser54 and Cys100 mutations, and their respective 2.8 and 3.3 Å distances to the carbonyl oxygen of HYA, indicated that Cys100 may form a hydrogen bond with the aldehyde group to stabilize the substrate, and that Ser54 may participate in a proton shuttle system during the reduction of substrate, instead of Ser54 forming polar interactions with a water molecule as reported recently by Srinivasan and Smolke.[8]

The docking results and the above site-mutation data prompted us to posit a simple catalytic mechanism for AbHDH: as observed in some zinc-dependent CAD or SAD families,[31] first a change in the conformation of AbHDH results in the catalytic Zn^{2+} establishing an electrostatic interaction with the aldehyde group of substrate HYA; then the *pro*-R hydride of NADPH is transferred from the C4 atom to the C1 atom of the aldehyde group in HYA; at this point, the hydroxyl group of Ser54 acts as a general acid, donating a proton to the Zn^{2+}-coordinated oxygen of HYA; and finally, the corresponding hyoscyamine is produced (Figure 5). In

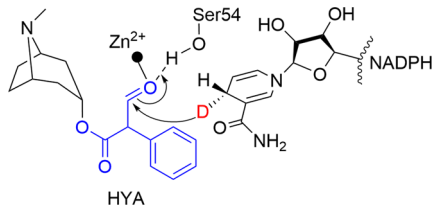

Figure 5. Proton shuttling mechanism proposed to operate during the reduction process in the active site of AbHDH. Solid arrows indicate the movement of two electrons between functional groups during the substrate reduction. The likely hydrogen bonds involved are shown as dashed lines.

order to determine which hydrogen of NADPH is responsible for hydride transfer, [4*S*-^{2}H] NADPH (Figure S9a) and [4*R*-^{2}H] (Figure S9b) NADPH were synthesized and used for AbHDH-catalyzed reactions. A GC-MS analysis revealed an incorporation of deuterium into phenylacetaldehyde only in the presence of [4*R*-^{2}H] NADPH but not with [4*S*-^{2}H] NADPH (Figure S10). Deuterated phenylethanol was separated by liquid chromatography and further identified by EI-HRMS (Figure S11). These results were consistent with the *pro*-R hydride of NADPH being used for the reduction reaction.

HDH Is Valuable for Promoting the Production of Pharmaceutical TAs in Planta. Since HDH was clearly able to reduce HYA to form hyoscyamine, we became interested in studying its relevance for engineering the production of hyoscyamine, anisodamine, and scopolamine in planta. To do so, root cultures of *A. belladonna*, in which *HDH* was overexpressed (driven by the CaMV 35S promoter, p35S), were established. PCR detection showed that the rooting gene (*rolB*) and the marker gene (*NPTII*) were both amplified from the positive control pBI121-HDH, control root lines, and *HDH*-overexpressing root lines. Fragments of *35S::HDH* (a genomic DNA from p35S to HDH) were specifically detected from the pBI121-HDH and *HDH*-overexpressing root lines yet not from the control root lines (Figure S12). Gene expression analysis, based on qPCR, indicated that the transcript levels of *HDH* were much higher in the *HDH*-overexpressing root lines than in the control root lines (Figure 6a). These results

https://dx.doi.org/10.1021/acscatal.0c04667
ACS Catal. 2021, 11, 2912−2924

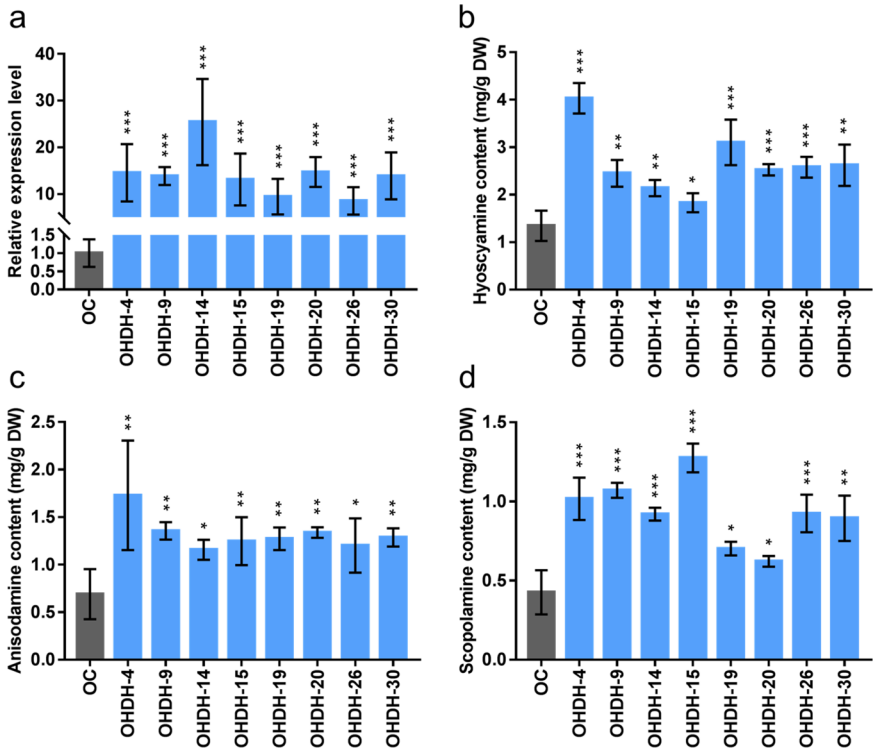

Figure 6. Effects of overexpression of *HDH* on the biosynthesis of TAs in root cultures of *A. belladonna*. (a) *HDH* expression levels in the root cultures. (b−d) Contents of alkaloids in the root cultures: (b) hyoscyamine, (c) anisodamine, and (d) scopolamine. DW, dry weight. OC, vector control root lines transformed with pBI121 vector. OHDH-4, 9, 14, 15, 19, 20, 26, 30 denote the representative *HDH*-overexpressing root cultures. The bars denote means ± standard deviations ($n \geq 3$). *, **, and *** indicate significant differences from control at the levels of $P < 0.05$, $P < 0.01$, and $P < 0.001$, respectively, as determined by *t* tests.

confirmed that the expression levels of *HDH* were substantially elevated in the *HDH*-overexpressing root lines.

The TA contents were determined in the root cultures of *A. belladonna*, by using LC-MS. The contents of hyoscyamine, anisodamine, and scopolamine were respectively 1.35 mg/g dry weight (DW), 0.69 mg/g DW, and 0.43 mg/g DW in the control root lines (Figure 6b−d). Hyoscyamine production was 1.83 to 4.03 mg/g DW in the HDH-overexpressing root lines (Figure 6b), suggesting that they could produce 35.56%−198.52% more hyoscyamine than could the control root lines. The anisodamine levels ranged from 1.16 to 1.73 mg/g DW in the HDH-overexpressing root lines (Figure 6c), while their scopolamine contents were slightly lower, at 0.62 to 1.28 mg/g DW (Figure 6d). These levels of anisodamine and scopolamine were also significantly higher in the HDH-overexpressing root lines than in the control root lines.

A few TA biosynthesis genes, namely *PMT*, *CYP80F1*, and *H6H*, have been used to engineer TA production in root cultures or plants. Overexpression of *PMT* markedly increased *N*-methylputrescine levels in *A. belladonna* and a *Duboisia* hybrid, but did not promote the biosynthesis of either hyoscyamine or scopolamine,[33,34] attributed to TA biosynthesis being limited downstream rather than at the PMT-catalyzed step.[33] Overexpression of *H6H* from *Hyoscyamus niger* markedly increased the scopolamine production in root cultures of *A. belladonna*, *H. niger*, and other TA-producing plants, and impressively, hyoscyamine was almost completely converted into scopolamine in leaves of *HnH6H*-overexpressing *A. belladonna* plants.[5,35−37] Overexpression of *CYP80F1*, whose product catalyzes the conversion of littorine to HYA, did not alter the overall production of hyoscyamine.[17] These metabolic engineering studies implied that it is worth trying to deploy some TA biosynthesis genes, such as HDH, in engineering hyoscyamine production in plants.

In this study, hyoscyamine production was significantly increased when *HDH* was overexpressed. Due to the resulting greater availability of hyoscyamine for H6H, the production of anisodamine and that of scopolamine were promoted as well. In contrast to the relatively low level of productivity in titers of hyoscyamine (around 80 μg/L) and scopolamine (around 30 μg/L) achieved by engineered yeast cells based on synthetic biology,[8] the productivity levels of hyoscyamine and scopolamine in engineered root cultures of *A. belladonna* were, respectively, 1.83−4.03 and 0.62−1.28 mg/g DW. For scopolamine in particular, its levels reached 1% DW in leaves of *HnH6H*-overexpressing *A. belladonna* plants.[35] Due to these results, and because commercial production of pharmaceutical TAs in engineered yeast needs their titer levels to be higher than 5 g/L,[8] we are confident that metabolic engineering of TA production in planta offers a promising way forward that can compete against synthetic-biology-based manufacturing of TAs in yeast cell factories. In fact, artemisinin is a prime example of this potential. Engineered yeast cells can produce artemisinin acid at a very high level (of about 25 g/L) and have been used to synthesize artemisinin at a relatively low cost.[38] The pharmaceutical company Sanofi S.A. had ambitiously declared a plan to launch the large-scale production of artemisinin using synthetic biology, back in 2013.[39] However, the marketplace did not cooperate with Sanofi's aspirations. The artemisinin generated via synthetic biology met market resistance because it still cost more than *Artemisia annua* plants cultivated by farmers,[40] such that today commercial production of

https://dx.doi.org/10.1021/acscatal.0c04667
ACS Catal. 2021, 11, 2912−2924

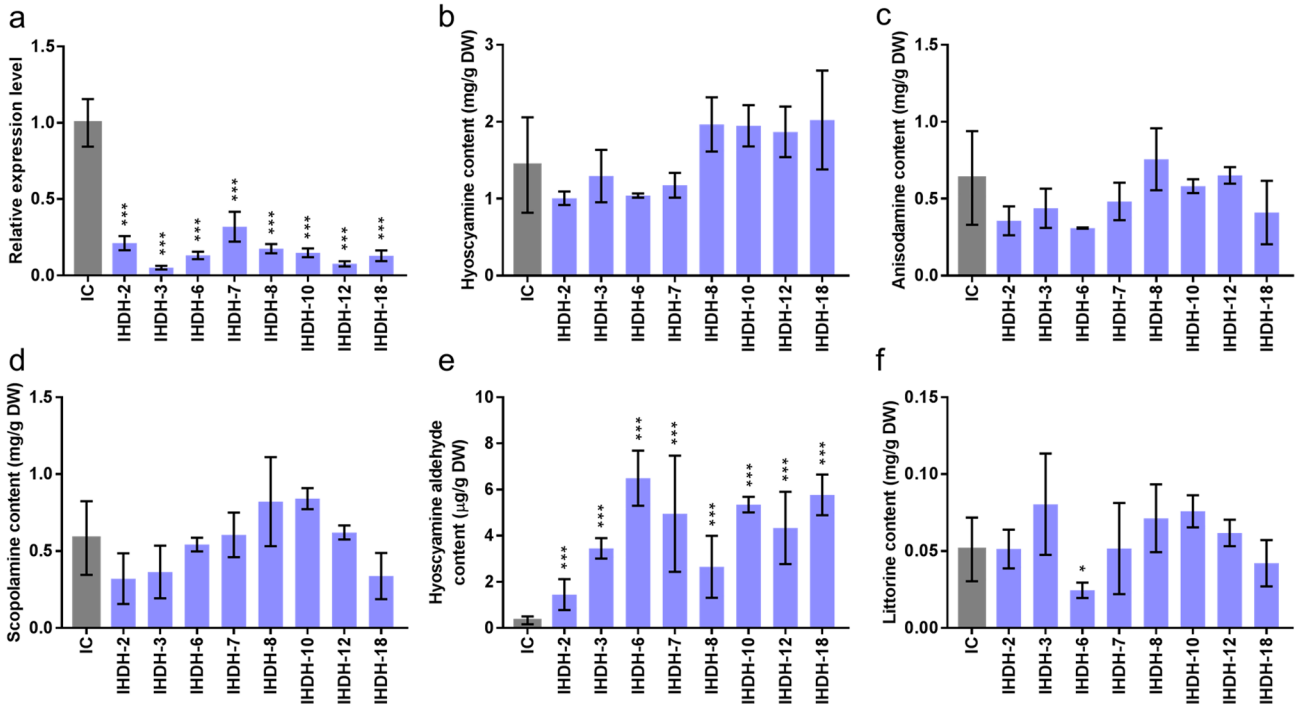

Figure 7. Effects of suppressing *HDH* on the biosynthesis of TAs in root cultures of *A. belladonna*. (a) *HDH* expression levels in the root cultures. (b–f) Contents of alkaloids in the root cultures: (b) hyoscyamine, (c) anisodamine, (d) scopolamine, (e) hyoscyamine aldehyde relative to the amount of hyoscyamine, and (f) littorine. DW, dry weight. IC, control root lines transformed with pBin19 vector. IHDH-2, 3, 6, 7, 8, 10, 12, and 18 denote the representative *HDH*-suppressing root cultures. The bars denote means ± standard deviations ($n \geq 3$). *, **, and *** indicate significant differences from the control at the levels of $P < 0.05$, $P < 0.01$, and $P < 0.001$, respectively, as determined by *t* tests.

artemisinin still depends on *A. annua* plants. Although microbial synthetic biology still represents a promising technology for manufacturing active pharmaceutical ingredients (APIs) with complicated structures, plant metabolic engineering might be considered at the present time to be a more promising way to produce some APIs.

HDH Is Replaceable for Hyoscyamine Formation in Planta. To further understand the role of HDH in hyoscyamine biosynthesis in planta, we established root cultures of *A. belladonna*, in which *HDH* was suppressed using RNAi technology. PCR detection confirmed the T-DNA harboring the HDH-RNAi fragment (driven by the 35S promoter) had been integrated into the genome of *A. belladonna* (Figure S12). The corresponding gene expression analysis showed that *HDH* transcript levels were markedly decreased in *HDH*-RNAi root lines (Figure 7a), indicating that *HDH* was substantially suppressed in transgenic root cultures of *A. belladonna*. Metabolite detection revealed, however, that the hyoscyamine (Figure 7b), anisodamine (Figure 7c), and scopolamine (Figure 7d) levels were not significantly altered when *HDH* was suppressed, demonstrating that suppression of *HDH* was not able to disrupt the formation of hyoscyamine. HYA was detected at relatively high levels in the *HDH*-RNAi root lines, but only so at trace levels in control root lines (Figure 7e); hence, suppression of *HDH* led to the accumulation of HYA. Littorine (Figure 7f) levels were not significantly increased when *HDH* was suppressed.

Generally, metabolite biosynthesis is disrupted when one or more key biosynthesis genes are suppressed or knocked out. For hyoscyamine, its production has been shown to be dramatically decreased, and in most cases the levels of candidate substrates significantly elevated, when certain TA biosynthesis genes were suppressed.[7,12,15,16,41] For example, when ArAT4 was suppressed, the levels of both phenylpyruvic acid (the direct product of the reaction catalyzed by ArAT4) and phenylalanine (the direct substrate for ArAT4) went unchanged, while the production of metabolites downstream of phenylpyruvic acid, including phenyllactic acid, hyoscyamine, and scopolamine, were each considerably reduced. This result was explained by the five other isozymes catalyzing the same reaction as ArAT4, and probably cell-specific expression of ArAT4, leading to functional redundancy with respect to the formation of phenylpyruvic acid.[15,16]

In the present study, since suppressing *HDH* did not decrease the production of hyoscyamine, anisodamine or scopolamine, it may be concluded that HDH is not essential for hyoscyamine to be formed in planta, and it is therefore reasonable to postulate that some other yet-to-be identified enzymes might complement the activity of HDH *in planta*. In fact, although hyoscyamine was produced, HYA was not detected in littorine-fed tobacco root cultures that expressed CYP80F1, which normally catalyzes littorine to form HYA.[17] Here we also used HDH to search tobacco transcriptomes and genomes, but could not find any HDH genes in tobacco (data not shown). Taken together, we may therefore deduce that some other enzymes in tobacco catalyze the reduction of HYA into hyoscyamine. Since the oxidoreductase family is large and composed of hundreds of members, others besides HDH might also be capable of reducing HYA to form hyoscyamine in planta. These yet-to-be identified enzymes that are able to reduce HYA to hyoscyamine await discovery and testing by scientists, to better understand and appreciate the complexity of the hyoscyamine biosynthesis process in planta.

https://dx.doi.org/10.1021/acscatal.0c04667
ACS Catal. 2021, 11, 2912–2924

CONCLUSIONS

Hyoscyamine dehydrogenase was identified from *A. belladonna*, and named AbHDH. Under physiological conditions in plant cells, AbHDH was concluded to mainly catalyze the reduction of hyoscyamine aldehyde to form hyoscyamine. The in vitro characterization and crystal structure of AbHDH to relatively high resolution revealed its catalytic mechanism and high affinity for substrates, which may allow for the syntheses of useful alcohols for the purpose of preparing complex natural products and pharmaceutical ingredients in future research. AbHDH was found to be a zinc-containing long-chain dehydrogenase, transferring the *pro*-R hydrogen from the 4-position of the NADPH cofactor. In addition, AbHDH was shown to be of value in engineering the production of pharmaceutical TAs in planta through an overexpression strategy.

EXPERIMENTAL SECTION

Gene Screen and Bioinformatics Analysis. The reduction of HYA to hyoscyamine is a typical reduction of an aldehyde, and many such reactions occur in biological settings and are catalyzed by alcohol dehydrogenase. Therefore, we speculated that alcohol dehydrogenase might catalyze HYA to produce hyoscyamine. To mine the members of the alcohol dehydrogenase family in an *A. belladonna* transcriptome database based on the Hidden Markov Model (PF08240), a clustering analysis was performed using the "pheatmap" package (to derive correlations between the expressions of various genes) in 'R' software. The corresponding phylogenetic tree was generated using the neighbor-joining method, in MEGA7 software.[42]

Cloning and Expression Analysis of HDH. The total RNA of *A. belladonna* secondary root tissue was isolated by using the RNAsimple Total RNA Kit (Tiangen, Beijing, China), after which a cDNA library for rapid amplification of cDNA ends (RACE) was constructed using the SMARTer RACE cDNA Amplification Kit according to its operational instructions (Clontech, CA, U.S.A.). The 3′-RACE and 5′-RACE of *HDH* were respectively carried out, according to the manufacturer's protocol. The full-length *HDH* was isolated by using a primer pair consisting of f-HDH-F and f-HDH-R, with amplification of the *HDH* gene carried out using HyPerFUsion DNA polymerase (APExBIO Technology, TX, USA). The ensuing PCR products were subcloned into a pJET1.2/blunt vector (Thermo Fisher Scientific, MA, USA) and sequenced. Tissue profiling of *HDH* was analyzed by carrying out qPCR, for which *PGK* served as the internal reference gene.[43] Secondary roots, primary roots, stems, and leaves of *A. belladonna* plants grown in the field for 4 months were harvested. The different tissues of *A. belladonna* were used for RNA isolation and cDNA synthesis, using kits from Tiangen Biotech (BJ, China), with SYBR qPCR Mix purchased from Novoprotein (SHH, China). The qPCR was performed using an IQ5 machine (Bio-Rad, CA, U.S.A.), which was also used to assess the expression levels of *HDH* in suppressed and overexpressed root cultures. All primers used in this study are listed in Table S3.

Isolation of the AbCYP80F1 Microsomal Protein and Determination of the HDH Catalytic Activity. The CYP80F1 coding sequence (CDS) was cloned into pYES2 with *Bam*HI and *Xho*I, and the resulting yeast expression vector was then transformed into the yeast strain WAT11. Transformants were selected on a synthetic dropout medium deficient in uracil with 2% glucose added. The microsomal protein of CYP80F1 was induced and isolated as previously described.[17,44] The HDH CDS was inserted into pET28a with *Eco*RI and *Xho*I, whose resulting vector was introduced into the *Escherichia coli* strain BL21 (DE3). The His-tagged HDH was induced and purified as described elsewhere.[16,45] For the HDH reduction activity assays, a reaction mixture (500 μL) containing 600 μg of microsomal protein, 5 mM NADPH, and 1 mM (*R*)-(−)-littorine in 100 mM potassium phosphate (pH 7.5) was made; the reaction was initiated by adding microsomal and HDH proteins (100 μg) and run at 30 °C for 12 h. Boiled HDH served as a negative control. For the HDH oxidation activity assays, a reaction mixture (500 μL) containing 2 mM NADP and 1 mM L-hyoscyamine in a 100 mM glycine buffer (pH 8.0) was made, and to this mixture was added the HDH protein (100 μg) to oxidize hyoscyamine, at 30 °C for 2 h (with boiled HDH used as a negative control). The oxidation and reduction reactions were each terminated by adding enough ammonium hydroxide to bring the final pH to a value of 10. The reaction mixtures were then added to Extrelut NT and incubated at room temperature for 30 min, after which the alkaloids were eluted with 20 mL of dichloromethane. A nitrogen stream was applied to remove the solvent, and the resulting residue was dissolved in 10 mL of methanol and immediately analyzed using LC-HRMS. Catalytic products were separated and detected using a Thermo Scientific Q Exactive mass spectrometer equipped with a Hypersil GOLD C18 column (100 × 2.1 mm, 1.9 μm; Thermo Scientific). The flow rate was set to 0.4 mL/min and the oven temperature was 35 °C. The samples were separated using a binary gradient elution with 0.1% formic acid in water (A) and acetonitrile (B). The corresponding elution procedures are described in Table S4. The injection volume was 2 μL. All measurements were taken using electron spray ionization (ESI) in its positive ion mode and full MS mode. Regarding the instrument parameters, sheath gas pressure was set at 35 psi, aux gas flow rate at 20 L/h, spray voltage at 3.00 kV, capillary temperature at 350 °C, S-lens RF level at 50, and aux gas heater temperature at 350 °C. The R-(−)-littorine standards were purchased from Toronto Research Chemicals (ON, Canada). The L-hyoscyamine standards were purchased from MCE (MedChemExpress, SHH, China).

Crystallization and Structure Determination of AbHDH. Crystals of AbHDH were grown using the hanging-drop vapor diffusion method at 293 K. The drops contained each a 1:1 mixture of 10 mg·ml^{-1} protein and a crystallization buffer (0.2 M ammonium sulfate, 0.1 M Tris-HCl [pH 8.0], 30% PEG 3350). Diffraction data were collected using X-rays at a wavelength of 0.9795 Å and a temperature of 100 K at beamline 18U of the Shanghai Synchrotron Radiation Facility (SSRF), and then processed using HKL3000 software.[46] The structure was determined by carrying out the molecular replacement method in Molrep based on using 1YQD[29] as the search model. An initial model was built using PHENIX.-autobuild[47] and subjected to manual adjustment using COOT,[48] with all models refined using PHENIX.refinement[47] and Refmac5.[49]

Molecular Docking of Substrate to AbHDH. Rigid molecular docking was performed using Autodock 4.2.[32] The ligand NADPH was downloaded from the PDB database (http://www.rcsb.org/) and docked into the cofactor-binding site of AbHDH. The ligands HYA and phenylacetaldehyde

https://dx.doi.org/10.1021/acscatal.0c04667
ACS Catal. 2021, 11, 2912−2924

were generated using ChemBio3D Ultra 12.0, and then energy minimized with Molecular Mechanics (MM2) until a minimum root-mean-square (RMS) gradient of 0.100 was achieved (https://www.chemdraw.com.cn/). When docking, the key parameters such as grid number and algorithm were set to default values, but rotatable bonds in the ligand were not set in this manner in order to allow for flexible docking. Finally, one hundred independent docking runs were performed, and the complex structure with the best combination of low binding energy and favorable orientation was selected. PyMOL 1.7 (http://www.pymol.org) was used for viewing the molecular interactions and image processing.

GC-MS Identification of the Products of Phenylacetaldehyde Reduction Mediated by AbHDH. Phenylacetaldehyde reduction reactions were carried out in 400 μL mixture containing potassium phosphate (100 mM, pH 7.0), 1 mM phenylacetaldehyde, 2 mM NADPH, and 50 μg of AbHDH. A similar reaction, but with preboiled AbHDH, was used as a negative control. These reactions were each initiated at 30 °C, and then stopped with an equal volume of 0.8 M formic acid after 3 h, extracted with 80 μL of ethyl acetate twice, and analyzed using GC-MS (GCMS-QP2010Plus, SHIMADZU, Kyoto, Japan). The MS analysis was carried out in electron ionization (EI) mode. Samples were separated using an Rtx-5 column (30 m × 0.25 mm × 0.25 μm, Restek) with a temperature gradient of 45 °C for 4 min, 45−185 °C at a rate of 14 °C/min, and 185 °C for 2 min.[50]

Analysis of Enzyme Kinetics Parameters and Equilibrium Constants. The five mutant HDH proteins, made with S54A, H74A, C100G, C100F, and C100Y substitutions, respectively, were each obtained by carrying out overlapping PCR. The primers used for this procedure are described in Table S3, and the corresponding proteins were purified by deploying essentially the same procedure used to purify the wild-type enzyme. The purified HDH protein (125 μg) was used in each oxidation/reduction enzymatic assay in 1 mL reaction buffers that contained 0.2 mM NADP-2Na/NADPH-4Na. Potassium phosphate buffer and glycine buffer (pH 4−12) were used to determine the optimal pH of HDH for its oxidation/reduction, and various temperatures (range: 25−50 °C) were tested to determine the optimum one for this oxidation/reduction, whose enzyme kinetics were then analyzed at these optimal pH and temperature conditions. Various concentrations of hyoscyamine (0.01−10 mM) and phenylacetaldehyde (0.01−3 mM) were used for the analysis of enzyme kinetics. The enzymatic activity was calculated based on NADPH consumption, which was spectrophotometrically followed at a wavelength of 340 nm (Thermo Scientific), and the K_m and V_{max} values were calculated from curve fitting of the Michaelis−Menten equation $v_0 = (V_{max} \times [S])/(K_m + [S])$. The k_{cat} values were calculated according to the equation $k_{cat} = V_{max}/[E]$. The standards for NADP-2Na, NADPH-4Na, and phenylacetaldehyde were purchased from Aladdin (SHH, China). Equilibrium constants of the reactions with hyoscyamine as the substrate were determined under various pH conditions (6.4, 7.2, and 10.4). Here, in each case, a reaction mixture containing 0.25 mM hyoscyamine and 0.25 mM $NADP^+$ was made, and then the reaction was monitored by measuring the (increase in) absorbance at 340 nm using an extinction coefficient of 6220 L M^{-1} cm^{-1} for NADPH. After equilibrium was reached, the concentration of product (hyoscyamine aldehyde) was calculated, to finally obtain the equilibrium constant (K_{eq}).[51]

Determination of the Stereospecificity of the Hydrogen Transfer from NADPH. [4*S*-^{2}H] NADPH and [4*R*-^{2}H] NADPH were synthesized according to the method reported by Barber[52] but with a slight modification. For [4*S*-^{2}H] NADPH, a reaction system (500 μL) containing 83 mM phosphate buffer (pH 8.0), 14.7 mM D-glucose-1-^{2}H, 9.3 mM $NADP^+$, 40% DMSO and 5 units of glucose-6-phosphate dehydrogenase (*Saccharomyces cerevisiae*) was made. For [4*R*-^{2}H] NADPH, a reaction system (500 μL) containing 25 mM Tris buffer (pH 9.0), 2.8 mM $NADP^+$, 1 M 2-propanol-$^2H_8$, and 5 units of alcohol dehydrogenase (*Thermoanaerobium brockii*) was made. Each of these reaction system was incubated at 30 °C for 1 h, and then 20 μL of the resulting reaction solution was added to an AbHDH reaction system including potassium phosphate (100 mM, pH 7.0), 1 mM phenylacetaldehyde, and 50 μg AbHDH. The enzymatic reaction was quenched by adding to it an equal volume of 0.8 M formic acid; the product was extracted twice using 80 μL of ethyl acetate, and analyzed using GC-MS. In order to further identify the deuterated phenylethanol, the amplification reaction of AbHDH catalysis was performed in a total volume of 2 mL. The organic phase was distilled to dryness under reduced pressure, and then the residues were dissolved in ethanol. Product of interest was isolated by HPLC and identified by EI-HRMS.

Establishment of Hairy Root Cultures and Molecular Detection. To investigate the functioning of *HDH* in the biosynthesis of TAs, overexpression or suppression of *HDH* and corresponding control root cultures were established according to published references.[7,37] All root cultures were identified by PCR using genomic DNA—including *rolB*, *NPTII*, *35S::HDH*, and *35S::HDH RNAi*—with qPCR used to confirm the expression levels of *HDH* in different root cultures (as described above). For the gene expression and metabolite analyses, root lines were cultured in liquid Murashige and Skoog (MS) medium for 28 days.[7,16] The primers used are listed in Table S3.

Metabolite Analysis of Root Cultures. Determination of littorine, hyoscyamine aldehyde, hyoscyamine, anisodamine, and scopolamine contents was done following Qiu et al.,[7] albeit with slight modifications. The harvested root cultures were lyophilized and ground into fine powder; 25 mg of this material was used for the metabolites' extraction and added to 1 mL of extraction buffer (20% methnol including 0.1% formic acid). Metabolites were extracted at 10 °C for 3 h and then immediately used for detection. To quantify the content of metabolites, chromatography and mass spectrometry were applied, using the same conditions as described above except the sampler was set as 4 °C. The injection volume was 5 μL after a 10-fold dilution. The standard curves of littorine, hyoscyamine, anisodamine, and scopolamine were built used authentic samples obtained from Toronto Research Chemicals and Sigma-Aldrich (MO, U.S.A.).

■ ASSOCIATED CONTENT

Supporting Information

The Supporting Information is available free of charge at https://pubs.acs.org/doi/10.1021/acscatal.0c04667.

Purified AbHDH, MS data for hyoscyamine and HYA, amino acid sequences alignment, HDH docked with phenylacetaldehyde, identification of reduction products of phenylacetaldehyde, optimal conditions for the

https://dx.doi.org/10.1021/acscatal.0c04667
ACS Catal. 2021, 11, 2912−2924

enzymatic reaction, MS data of synthesized [4-^{2}H] NADPH, MS data for deuterium exchange experiments, MS data for deuterated phenylethanol, genomic DNA detection, candidate HDH genes, X-ray crystallography data collection, primers used in the study, and mobile phase gradient (PDF)

AUTHOR INFORMATION

Corresponding Authors

Sheng-Xiong Huang − *State Key Laboratory of Phytochemistry and Plant Resources in West China, and CAS Center for Excellence in Molecular Plant Sciences, Kunming Institute of Botany, Chinese Academy of Sciences, Kunming 650201, China;* orcid.org/0000-0002-3616-8556; Email: sxhuang@mail.kib.ac.cn

Zhihua Liao − *Chongqing Key Laboratory of Plant Resource Conservation and Germplasm Innovation, Key Laboratory of Eco-environments in Three Gorges Reservoir Region (Ministry of Education), SWU-TAAHC Medicinal Plant Joint R&D Centre, School of Life Sciences, Southwest University, Chongqing 400715, China;* orcid.org/0000-0002-1283-4649; Email: zhliao@swu.edu.cn

Authors

Fei Qiu − *Chongqing Key Laboratory of Plant Resource Conservation and Germplasm Innovation, Key Laboratory of Eco-environments in Three Gorges Reservoir Region (Ministry of Education), SWU-TAAHC Medicinal Plant Joint R&D Centre, School of Life Sciences, Southwest University, Chongqing 400715, China*

Yijun Yan − *State Key Laboratory of Phytochemistry and Plant Resources in West China, and CAS Center for Excellence in Molecular Plant Sciences, Kunming Institute of Botany, Chinese Academy of Sciences, Kunming 650201, China*

Junlan Zeng − *Chongqing Key Laboratory of Plant Resource Conservation and Germplasm Innovation, Key Laboratory of Eco-environments in Three Gorges Reservoir Region (Ministry of Education), SWU-TAAHC Medicinal Plant Joint R&D Centre, School of Life Sciences, Southwest University, Chongqing 400715, China*

Jian-Ping Huang − *State Key Laboratory of Phytochemistry and Plant Resources in West China, and CAS Center for Excellence in Molecular Plant Sciences, Kunming Institute of Botany, Chinese Academy of Sciences, Kunming 650201, China*

Lingjiang Zeng − *Chongqing Key Laboratory of Plant Resource Conservation and Germplasm Innovation, Key Laboratory of Eco-environments in Three Gorges Reservoir Region (Ministry of Education), SWU-TAAHC Medicinal Plant Joint R&D Centre, School of Life Sciences, Southwest University, Chongqing 400715, China*

Wei Zhong − *State Key Laboratory of Phytochemistry and Plant Resources in West China, and CAS Center for Excellence in Molecular Plant Sciences, Kunming Institute of Botany, Chinese Academy of Sciences, Kunming 650201, China*

Xiaozhong Lan − *TAAHC-SWU Medicinal Plant Joint R&D Centre, Tibetan Collaborative Innovation Centre of Agricultural and Animal Husbandry Resources, Xizang Agricultural and Animal Husbandry College, Nyingchi of Tibet 860000, China*

Min Chen − *College of Pharmaceutical Sciences, Key Laboratory of Luminescent and Real-Time Analytical Chemistry (Ministry of Education), Southwest University, Chongqing 400715, China*

Complete contact information is available at: https://pubs.acs.org/10.1021/acscatal.0c04667

Author Contributions

$^{\perp}$F.Q., Y.Y., and J.Z. contributed equally to this work.

Notes

The authors declare no competing financial interest.

ACKNOWLEDGMENTS

This work is financially supported by the fundings listed below: the NSFC projects (U1902212, 31770335 and 32000239), the National Key R&D Program of China (2018YFA0900600), the National Transgenic Major Project of China (2019ZX08010-004), the Forth National Survey of Traditional Chinese Medicine Resources, Chinese or Tibet Medicinal Resources Investigation in Tibet Autonomous Region (State Administration of Chinese Traditional Medicine 20191217-540124, 20191223-550126, and 20200501-542329), China Postdoctoral Science Foundation (2020M683216), Key Research Program of Frontier Sciences and the Strategic Priority Research Program, CAS (XDB27020205 and QYZDB-SSW-SMC051), and foundations from Yunnan province (2019FJ007, 2019ZF011-2, and 2019FA034). The study on the HDH enzyme has been included in an authorized patent (ZL 201910826205.8) and a PCT patent application (PCT/CN2020/113138) made by Southwest University.

REFERENCES

(1) Kohnen-Johannsen, K.; Kayser, O. Tropane Alkaloids: Chemistry, Pharmacology, Biosynthesis and Production. *Molecules* **2019**, *24*, 796.

(2) Yamada, Y.; Tabata, M. Plant Biotechnology of Tropane Alkaloids. *Plant Biotechnol.* **1997**, *14*, 1−10.

(3) Grynkiewicz, G.; Gadzikowska, M. Tropane Alkaloids as Medicinally Useful Natural Products and Their Synthetic Derivatives as New Drugs. *Pharmacol. Reports* **2008**, *60*, 439−463.

(4) Ullrich, S. F.; Hagels, H.; Kayser, O. Scopolamine: A Journey from the Field to Clinics. *Phytochem. Rev.* **2017**, *16*, 333−353.

(5) Xia, K.; Liu, X.; Zhang, Q.; Qiang, W.; Guo, J.; Lan, X.; Chen, M.; Liao, Z. Promoting Scopolamine Biosynthesis in Transgenic *Atropa belladonna* Plants with pmt and h6h Overexpression under Field Conditions. *Plant Physiol. Biochem.* **2016**, *106*, 46−53.

(6) Humphrey, A. J.; O'Hagan, D. Tropane Alkaloid Biosynthesis. A Century Old Problem Unresolved. *Nat. Prod. Rep.* **2001**, *18*, 494−502.

(7) Qiu, F.; Zeng, J.; Wang, J.; Huang, J.; Zhou, W.; Yang, C.; Lan, X.; Chen, M.; Huang, S.; Kai, G.; Liao, Z. Functional Genomics Analysis Reveals Two Novel Genes Required for Littorine Biosynthesis. *New Phytol.* **2020**, *225*, 1906−1914.

(8) Srinivasan, P.; Smolke, C. D. Biosynthesis of Medicinal Tropane Alkaloids in Yeast. *Nature* **2020**, *585*, 614−619.

(9) Zhao, T.; Li, S.; Wang, J.; Zhou, Q.; Yang, C.; Bai, F.; Lan, X.; Chen, M.; Liao, Z. Engineering Tropane Alkaloid Production Based on Metabolic Characterization of Ornithine Decarboxylase in *Atropa belladonna*. *ACS Synth. Biol.* **2020**, *9*, 437−448.

(10) Hashimoto, T.; Yukimune, Y.; Yamada, Y. Putrescine and Putrescine *N*-methyltransferase in the Biosynthesis of Tropane Alkaloids in Cultured Roots of *Hyoscyamus albus*. *Planta* **1989**, *178*, 131−137.

(11) Katoh, A.; Shoji, T.; Hashimoto, T. Molecular Cloning of *N*-methylputrescine Oxidase from Tobacco. *Plant Cell Physiol.* **2007**, *48*, 550−554.
(12) Bedewitz, M. A.; Jones, A. D.; D'Auria, J. C.; Barry, C. S. Tropinone Synthesis via an Atypical Polyketide Synthase and P450-Mediated Cyclization. *Nat. Commun.* **2018**, *9*, 5281.
(13) Huang, J.-P.; Fang, C.; Ma, X.; Wang, L.; Yang, J.; Luo, J.; Yan, Y.; Zhang, Y.; Huang, S.-X. Tropane Alkaloids Biosynthesis Involves an Unusual Type III Polyketide Synthase and Non-enzymatic Condensation. *Nat. Commun.* **2019**, *10*, 4036.
(14) Dräger, B. Tropinone Reductases, Enzymes at the Branch Point of Tropane Alkaloid Metabolism. *Phytochemistry* **2006**, *67*, 327−337.
(15) Bedewitz, M. A.; Gongora-Castillo, E.; Uebler, J. B.; Gonzales-Vigil, E.; Wiegert-Rininger, K. E.; Childs, K. L.; Hamilton, J. P.; Vaillancourt, B.; Yeo, Y.-S.; Chappell, J.; DellaPenna, D.; Jones, A. D.; Buell, C. R.; Barry, C. S. A Root-expressed L-Phenylalanine:4-Hydroxyphenylpyruvate Aminotransferase Is Required for Tropane Alkaloid Biosynthesis in *Atropa belladonna*. *Plant Cell* **2014**, *26*, 3745−3762.
(16) Qiu, F.; Yang, C.; Yuan, L.; Xiang, D.; Lan, X.; Chen, M.; Liao, Z. A Phenylpyruvic Acid Reductase Is Required for Biosynthesis of Tropane Alkaloids. *Org. Lett.* **2018**, *20*, 7807−7810.
(17) Li, R.; Reed, D. W.; Liu, E.; Nowak, J.; Pelcher, L. E.; Page, J. E.; Covello, P. S. Functional Genomic Analysis of Alkaloid Biosynthesis in *Hyoscyamus niger* Reveals a Cytochrome P450 Involved in Littorine Rearrangement. *Chem. Biol.* **2006**, *13*, 513−520.
(18) O'Hagan, D.; Robins, R. Tropic Acid Ester Biosynthesis in *Datura stramonium* and Related Species. *Chem. Soc. Rev.* **1998**, *27*, 207.
(19) Nasomjai, P.; Reed, D. W.; Tozer, D. J.; Peach, M. J. G.; Slawin, A. M. Z.; Covello, P. S.; O'Hagan, D. Mechanistic Insights into the Cytochrome P450-mediated Oxidation and Rearrangement of Littorine in Tropane Alkaloid Biosynthesis. *ChemBioChem* **2009**, *10*, 2382−2393.
(20) Liao, Z.; Chen, M.; Yang, C.; Qiu, F.; Zeng, J. Hyoscyamine aldehyde reductase and use of thereof. China Patent, ZL201910826205.8, 2019.
(21) Hashimoto, T.; Matsuda, J.; Yamada, Y. Two-Step Epoxidation of Hyoscyamine to Scopolamine Is Catalyzed by Bifunctional Hyoscyamine 6*β*-Hydroxylase. *FEBS Lett.* **1993**, *329*, 35−39.
(22) Li, J.; van Belkum, M. J.; Vederas, J. C. Functional Characterization of Recombinant Hyoscyamine 6*β*-Hydroxylase from *Atropa belladonna*. *Bioorg. Med. Chem.* **2012**, *20*, 4356−4363.
(23) Sandala, G. M.; Smith, D. M.; Radom, L. The Carbon-Skeleton Rearrangement in Tropane Alkaloid Biosynthesis. *J. Am. Chem. Soc.* **2008**, *130*, 10684−10690.
(24) Suzuki, K.; Yun, D. J.; Chen, X. Y.; Yamada, Y.; Hashimoto, T. An *Atropa belladonna* Hyoscyamine 6beta-Hydroxylase Gene is Differentially Expressed in the Root Pericycle and Anthers. *Plant Mol. Biol.* **1999**, *40*, 141−152.
(25) Kandel, S.; Sauveplane, V.; Compagnon, V.; Franke, R.; Millet, Y.; Schreiber, L.; Werck-Reichhart, D.; Pinot, F. Characterization of a Methyl Jasmonate and Wounding-Responsive Cytochrome P450 of *Arabidopsis thaliana* Catalyzing Dicarboxylic Fatty Acid Formation in Vitro. *FEBS J.* **2007**, *274*, 5116−5127.
(26) Biazzi, E.; Carelli, M.; Tava, A.; Abbruscato, P.; Losini, I.; Avato, P.; Scotti, C.; Calderini, O. CYP72A67 Catalyzes a Key Oxidative Step in *Medicago truncatula* Hemolytic Saponin Biosynthesis. *Mol. Plant* **2015**, *8*, 1493−1506.
(27) Zhao, Q.; Zhang, Y.; Wang, G.; Hill, L.; Weng, J. K.; Chen, X. Y.; Xue, H.; Martin, C. A Specialized Flavone Biosynthetic Pathway Has Evolved in the Medicinal Plant, *Scutellaria baicalensis*. *Sci. Adv.* **2016**, *2*, e1501780.
(28) Stavrinides, A.; Tatsis, E. C.; Caputi, L.; Foureau, E.; Stevenson, C. E. M.; Lawson, D. M.; Courdavault, V.; O'Connor, S. E. Structural Investigation of Heteroyohimbine Alkaloid Synthesis Reveals Active Site Elements That Control Stereoselectivity. *Nat. Commun.* **2016**, *7*, 1−14.
(29) Bomati, E. K.; Noel, J. P. Structural and Kinetic Basis for Substrate Selectivity in *Populus tremuloides* Sinapyl Alcohol Dehydrogenase. *Plant Cell* **2005**, *17*, 1598−1611.
(30) Youn, B.; Camacho, R.; Moinuddin, S. G. A.; Lee, C.; Davin, L. B.; Lewis, N. G.; Kang, C. Crystal Structures and Catalytic Mechanism of the *Arabidopsis* Cinnamyl Alcohol Dehydrogenases AtCAD5 and AtCAD4. *Org. Biomol. Chem.* **2006**, *4*, 1687−1697.
(31) Jun, S.-Y.; Walker, A. M.; Kim, H.; Ralph, J.; Vermerris, W.; Sattler, S. E.; Kang, C. The Enzyme Activity and Substrate Specificity of Two Major Cinnamyl Alcohol Dehydrogenases in *Sorghum* (*Sorghum bicolor*), SbCAD2 and SbCAD4. *Plant Physiol.* **2017**, *174*, 2128−2145.
(32) Forli, S.; Huey, R.; Pique, M. E.; Sanner, M. F.; Goodsell, D. S.; Olson, A. J. Computational Protein−Ligand Docking and Virtual Drug Screening with the AutoDock Suite. *Nat. Protoc.* **2016**, *11*, 905−919.
(33) Moyano, E.; Fornalé, S.; Palazón, J.; Cusidó, R. M.; Bagni, N.; Piñol, M. T. Alkaloid Production in *Duboisia* hybrid Hairy Root Cultures Overexpressing the pmt Gene. *Phytochemistry* **2002**, *59*, 697−702.
(34) Rothe, G.; Hachiya, A.; Yamada, Y.; Hashimoto, T.; Dräger, B. Alkaloids in Plants and Root Cultures of *Atropa belladonna* Overexpressing Putrescine *N*-methyltransferase. *J. Exp. Bot.* **2003**, *54*, 2065−2070.
(35) Yun, D.-J. J.; Hashimoto, T.; Yamada, Y. Metabolic Engineering of Medicinal Plants: Transgenic *Atropa belladonna* with an Improved Alkaloid Composition. *Proc. Natl. Acad. Sci. U. S. A.* **1992**, *89*, 11799−11803.
(36) Zhang, L.; Ding, R.; Chai, Y.; Bonfill, M.; Moyano, E.; Oksman-Caldentey, K.-M.; Xu, T.; Pi, Y.; Wang, Z.; Zhang, H.; Kai, G.; Liao, Z.; Sun, X.; Tang, K. Engineering Tropane Biosynthetic Pathway in *Hyoscyamus niger* Hairy Root Cultures. *Proc. Natl. Acad. Sci. U. S. A.* **2004**, *101*, 6786−6791.
(37) Lan, X.; Zeng, J.; Liu, K.; Zhang, F.; Bai, G.; Chen, M.; Liao, Z.; Huang, L. Comparison of Two Hyoscyamine 6*β*-Hydroxylases in Engineering Scopolamine Biosynthesis in Root Cultures of *Scopolia lurida*. *Biochem. Biophys. Res. Commun.* **2018**, *497*, 25−31.
(38) Paddon, C. J.; Westfall, P. J.; Pitera, D. J.; Benjamin, K.; Fisher, K.; McPhee, D.; Leavell, M. D.; Tai, A.; Main, A.; Eng, D.; Polichuk, D. R.; Teoh, K. H.; Reed, D. W.; Treynor, T.; Lenihan, J.; Jiang, H.; Fleck, M.; Bajad, S.; Dang, G.; Dengrove, D.; Diola, D.; Dorin, G.; Ellens, K. W.; Fickes, S.; Galazzo, J.; Gaucher, S. P.; Geistlinger, T.; Henry, R.; Hepp, M.; Horning, T.; Iqbal, T.; Kizer, L.; Lieu, B.; Melis, D.; Moss, N.; Regentin, R.; Secrest, S.; Tsuruta, H.; Vazquez, R.; Westblade, L. F.; Xu, L.; Yu, M.; Zhang, Y.; Zhao, L.; Lievense, J.; Covello, P. S.; Keasling, J. D.; Reiling, K. K.; Renninger, N. S.; Newman, J. D. High-Level Semi-Synthetic Production of the Potent Antimalarial Artemisinin. *Nature* **2013**, *496*, 528−532.
(39) D'Oca, G. Sanofi to launch large-scale production of artemisinin. *Pharm. Bioprocess* **2013**, *1*, 137−139.
(40) Peplow, M. Synthetic Biology's First Malaria Drug Meets Market Resistance. *Nature* **2016**, *530*, 389−390.
(41) Geng, C.; Zhao, T.; Yang, C.; Zhang, Q.; Bai, F.; Zeng, J.; Zhang, F.; Liu, X.; Lan, X.; Chen, M.; Liao, Z. Metabolic Characterization of *Hyoscyamus niger* Root-Specific Putrescine *N*-methyltransferase. *Plant Physiol. Biochem.* **2018**, *127*, 47−54.
(42) Kumar, S.; Stecher, G.; Tamura, K. MEGA7: Molecular Evolutionary Genetics Analysis Version 7.0 for Bigger Datasets. *Mol. Biol. Evol.* **2016**, *33*, 1870−1874.
(43) Li, J.; Chen, M.; Qiu, F.; Qin, B.; Liu, W.; Wu, N.; Lan, X.; Wang, Q.; Liao, Z.; Tang, K. Reference Gene Selection for Gene Expression Studies Using Quantitative Real-Time PCR Normalization in *Atropa belladonna*. *Plant Mol. Biol. Rep.* **2014**, *32*, 1002−1014.
(44) Katavic, V.; Mietkiewska, E.; Barton, D. L.; Giblin, E. M.; Reed, D. W.; Taylor, D. C. Restoring Enzyme Activity in Nonfunctional Low Erucic Acid *Brassica napus* Fatty Acid Elongase 1 by a Single Amino Acid Substitution. *Eur. J. Biochem.* **2002**, *269*, 5625−5631.
(45) Liao, Z.; Qiu, F.; Zeng, J.; Gu, L.; Wang, B.; Lan, X.; Chen, M. A Novel UDP-Glycosyltransferase of *Rhodiola crenulata* Converts

Tyrosol to Specifically Produce Icariside D2. *BioMed Res. Int.* **2018**, *2018*, 1−8.
(46) Minor, W.; Cymborowski, M.; Otwinowski, Z.; Chruszcz, M. HKL −3000: The Integration of Data Reduction and Structure Solution − from Diffraction Images to an Initial Model in Minutes. *Acta Crystallogr., Sect. D: Biol. Crystallogr.* **2006**, *62*, 859−866.
(47) Adams, P. D.; Afonine, P. V.; Bunkóczi, G.; Chen, V. B.; Davis, I. W.; Echols, N.; Headd, J. J.; Hung, L.-W.; Kapral, G. J.; Grosse-Kunstleve, R. W.; McCoy, A. J.; Moriarty, N. W.; Oeffner, R.; Read, R. J.; Richardson, D. C.; Richardson, J. S.; Terwilliger, T. C.; Zwart, P. H. PHENIX : A Comprehensive Python-Based System for Macromolecular Structure Solution. *Acta Crystallogr., Sect. D: Biol. Crystallogr.* **2010**, *66*, 213−221.
(48) Emsley, P.; Lohkamp, B.; Scott, W. G.; Cowtan, K. Features and Development of Coot. *Acta Crystallogr., Sect. D: Biol. Crystallogr.* **2010**, *66*, 486−501.
(49) Murshudov, G. N.; Skubák, P.; Lebedev, A. A.; Pannu, N. S.; Steiner, R. A.; Nicholls, R. A.; Winn, M. D.; Long, F.; Vagin, A. A. REFMAC 5 for the Refinement of Macromolecular Crystal Structures. *Acta Crystallogr., Sect. D: Biol. Crystallogr.* **2011**, *67*, 355−367.
(50) Torrens-Spence, M. P.; Pluskal, T.; Li, F.-S.; Carballo, V.; Weng, J.-K. Complete Pathway Elucidation and Heterologous Reconstitution of *Rhodiola* Salidroside Biosynthesis. *Mol. Plant* **2018**, *11*, 205−217.
(51) Bessette, P. H.; Cotto, J. J.; Gilbert, H. F.; Georgiou, G. In Vivo and in Vitro Function of The *Escherichia Coli* Periplasmic Cysteine Oxidoreductase DsbG. *J. Biol. Chem.* **1999**, *274*, 7784−7792.
(52) Pollock, V. V.; Barber, M. J. Kinetic and Mechanistic Properties of Biotin Sulfoxide Reductase. *Biochemistry* **2001**, *40*, 1430−1440.

https://dx.doi.org/10.1021/acscatal.0c04667
ACS Catal. 2021, 11, 2912−2924